



Maosheng Zheng · Mingbo Tong · JianPing Chen · Le Li

# A new locking-free beam element based on absolute nodal coordinates

Received: 17 August 2023 / Revised: 16 September 2023 / Accepted: 21 September 2023 / Published online: 21 October 2023  
© The Author(s), under exclusive licence to Springer-Verlag GmbH Austria, part of Springer Nature 2023

**Abstract** In this paper, a novel locking-free finite beam element is proposed utilizing the absolute nodal coordinate formulation. By incorporating a gradient vector along the transverse direction at the boundary points, the linear interpolation of the gradient vector field within this element is achieved. Consequently, the problem of constant transverse strain distribution, which is observed in the Omar–Shabana beam element, is effectively addressed. Building upon this concept, this study further extends the proposed element from two dimensions to three dimensions. Additionally, it analyzes and compares the locking alleviation mechanism of the newly developed element and Patel–Shabana beam element. The analysis aims to provide insights into the factors contributing to the locking alleviation of different absolute nodal coordinate formulation (ANCF) elements. Furthermore, to demonstrate the effectiveness of the new element, six numerical simulation examples are designed, comprising three and three dynamic examples. These examples encompass small deformation statics, large deformation statics, small-scale motion, large-scale motion, and rotational motion problems. Finally, the results indicate that the proposed ANCF beam element can effectively alleviate the locking problem. The element exhibits robust adaptability, rationality, and effectiveness when subjected to complex mechanical characteristics by comparing the numerical results of this element with the classical Omar–Shabana, high-order Shen, and Patel–Shabana elements.

## 1 Introduction

The absolute nodal coordinate formulation [1, 2] (ANCF) was a new FE formulation proposed by Shabana [3] in the 1990s. The proposed method employs the unified interpolation field functions to depict the displacement of the material points along the beam, whereas the gradient vector is used to represent the beam's orientation, replacing the traditional rotation angle parameters. This approach effectively resolves the large deformation problem of a flexible beam within a non-incremental solution framework. Moreover, this method offers several the advantages, including a constant mass matrix and the absence of Coriolis and centrifugal forces [3]. Over the past two decades, the ANCF has found extensive utilization in diverse engineering applications. Examples include the modeling of high-speed pantograph–catenary systems, recovery of tethered satellites, and deployment of thin-film solar sails.

M. Zheng · M. Tong (✉) · J. Chen · L. Li  
College of Aerospace Engineering, Nanjing University of Aeronautics and Astronautics (NCAA), Nanjing 210016, China  
e-mail: 3201386601@qq.com

M. Zheng  
e-mail: issaczms@nuaa.edu.cn

J. Chen  
e-mail: jpchen@nuaa.edu.cn

L. Li  
e-mail: ll01002@nuaa.edu.cn

However, similar to traditional finite elements, the ANCF beam elements are also susceptible to the occurrence of locking phenomenon. An illustrative example is the study of the Omar–Shabana [4] beam element. García-Vallejo et al. [5] comprehensively elucidated the mechanism of curvature thickness locking and shear locking, focusing on the kinematics aspects. They identified the occurrence of Poisson locking arises from the inconsistency between the higher-order interpolation in the axial direction and the lower-order interpolation in the transverse direction. This inconsistency leads to stress coupling in different directions, resulting in the generation of pseudo-stresses during the bending process. Consequently, the displacement response of the beam element is significantly underestimated compared to actual solution. Therefore, researchers have been actively investigating methods to mitigate the detrimental influences of locking on these elements.

Sopanen and Mikkola [6] artificially set Poisson's ratio of 0 to alleviate the issue of Poisson locking, but this approach deviates from the actual conditions. García-Vallejo et al. [5] proposed a new two-dimensional shear deformation ANCF beam element with the reduced integral technique, which effectively alleviated the element's locking phenomenon. Gerstmayr [7–9] and Matikainen [7] only considered the Poisson effect in the axial direction of the beam and reconstructed the elastic force matrix of the elements with reduced integration, which effectively mitigate Poisson locking. Mikkola et al. [10] adopted independent interpolation for lateral deformation to better capture the Poisson effect on the elements. Schwab and Meijaard [11] used the elastic line method to reconstruct the elastic force formulation, which eliminated the high-order coupling terms of the axial and lateral deformation and alleviated Poisson locking. Additionally, Schwab and Meijaard [11] used the Hellinger–Reissner variational principle to alleviate the shear locking of three-dimensional full-parameter ANCF beam elements. Nachbagauer et al. [12, 13] used enhanced continuum mechanics formulation to alleviate elements' locking. Shen et al. [14, 15] developed a series of higher-order beam elements utilizing Pascal trigonometric polynomials. These elements employ a greater number of generalized coordinates and more complex interpolation functions. Hence, they are capable of accurately capturing many structural deformations, including cross section warping deformations. Patel and Shabana [16–18] decoupled high-order coupling terms from element kinematics and proposed a new method, called strain split method [19–22], to alleviate Poisson locking. Additionally, Patel and Shabana developed a new higher-order two-dimensional ANCF beam element [17], which can also effectively alleviate Poisson locking.

The remainder of this paper is arranged as follows. Section 2 reviews the classical Omar–Shabana ANCF beam element and presents a detailed analysis of the underlying causes of Poisson locking. Section 3 introduces a new planar two-dimensional ANCF beam element developed in this study, which can alleviate the locking phenomenon without reducing integral or modifying elastic force formulation. Section 4 presents a high-order two-dimensional ANCF beam element developed by Patel and Shabana. Further, two different ideas to alleviate Poisson locking are obtained by comparing them with the element presented in Sect. 3. Section 5 extends the plane element developed in Sect. 3 to a three-dimensional space, and a more generalized ANCF beam element is obtained. Section 6 compares and investigates the performance of several elements, including the element developed in this study through a series of numerical examples of statics and dynamics, proving that the developed element can effectively alleviate Poisson locking and has good accuracy and convergence. Finally, the conclusion is presented in Sect. 7.

## 2 Omar–Shabana ANCF beam element

The Omar–Shabana beam element is a two-dimensional shear deformable ANCF finite element. The spatial coordinates of any material point in the element can be described using the position vector and two gradient vectors associated with the element nodes (Fig. 1), which can capture the stretching, bending, and shearing deformation of a flexible beam.

In Fig. 1, the two nodes are located on the central axis of the beam ( $X = 0$  and  $X = L$  defined the material coordinates of the two nodes in the material coordinate system). Here,  $\mathbf{r}$  represents the position vector, and  $\mathbf{r}_x$  and  $\mathbf{r}_y$  represent two gradient vectors, respectively. The generalized coordinates array of this element can be defined as follows:

$$\mathbf{q} = [\mathbf{r}^T(0) \mathbf{r}_X^T(0) \mathbf{r}_Y^T(0) \mathbf{r}(L) \mathbf{r}_X^T(L) \mathbf{r}_Y^T(L)]^T. \quad (1)$$

The interpolation functions used to describe the spatial position of material points can be defined as

$$\mathbf{r} = \begin{bmatrix} x \\ y \end{bmatrix} = \begin{bmatrix} a_0 + a_1 X + a_2 Y + a_3 XY + a_4 X^2 + a_5 X^3 \\ b_0 + b_1 X + b_2 Y + b_3 XY + b_4 X^2 + b_5 X^3 \end{bmatrix}, \quad (2)$$

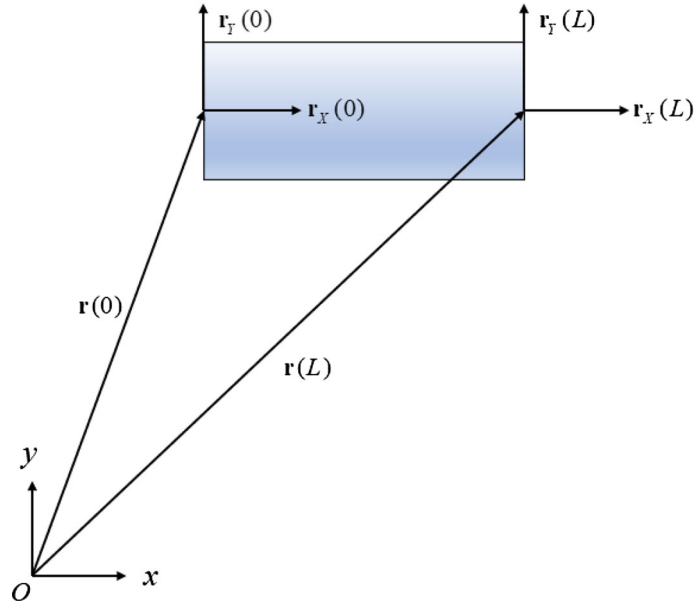


Fig. 1 Omar–Shabana beam element

where  $X$  and  $Y$  represent the material coordinates of the points in the beam. Further, the generalized coordinates are used to describe the position of points; hence, Eq. (2) can be rewritten as follows:

$$\mathbf{r} = [S_1\mathbf{I} \ S_2\mathbf{I} \ S_3\mathbf{I} \ S_4\mathbf{I} \ S_5\mathbf{I} \ S_6\mathbf{I}]\mathbf{q}, \quad (3)$$

where  $S_1 \sim S_6$  can be expressed as

$$\begin{aligned} S_1 &= 1 - 3\xi^2 + 2\xi^3 \\ S_2 &= L(\xi - 2\xi^2 + \xi^3) \\ S_3 &= h(1 - \xi)\eta \\ S_4 &= 3\xi^2 - 2\xi^3 \\ S_5 &= L(-\xi^2 + \xi^3) \\ S_6 &= h\xi\eta. \end{aligned} \quad (4)$$

Here,  $L$  and  $h$  denote the length and height of the element, respectively, and  $\xi = \frac{X}{L}$ ,  $\eta = \frac{Y}{h}$ .

The transverse strain of the element at  $X = 0$  can be expressed as

$$\varepsilon_y = \frac{1}{2}(\|\mathbf{r}_Y(0)\|_2^2 - 1). \quad (5)$$

Note that the distribution of  $\varepsilon_y$  along the cross-sectional direction remains constant, which does not conform to the distribution of transverse strain of the beam element under bending deformation. This inconsistency in distribution leads to locking phenomena in the beam element.

The transverse strain of element can be expressed as

$$\varepsilon_y = \frac{1}{2}((\xi - 1)^2\|\mathbf{r}_Y(0)\|_2^2 + \xi^2\|\mathbf{r}_Y(L)\|_2^2 - 1) - \xi(\xi - 1)\mathbf{r}_Y^T(0)\mathbf{r}_Y(L). \quad (6)$$

According to Eq. (6), the distribution of  $\varepsilon_y$  follows a quadratic function along the beam axis. However, due to the lower-order lateral interpolation, the transverse strain  $\varepsilon_y$  is only a function that has the independent variable  $X$  and time. Consequently, the nodes and the interior of the element both suffer from the Poisson locking. Therefore, it is an important idea to design a reasonable interpolation function to ensure an accurate distribution of transverse strain  $\varepsilon_y$  along the cross section.

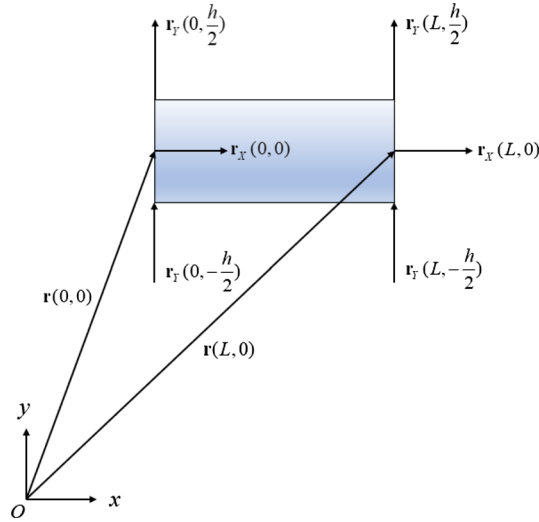


**Fig. 2** New two-dimensional ANCF beam element

### 3 New two-dimensional shear deformable ANCF beam element

#### 3.1 Element kinematics

One method to alleviate Poisson's locking is to increase the order of transverse interpolation, which allows for better capturing of the telescopic effect of cross section. In this study, a new beam element is proposed to investigate its performance in alleviating locking. Figure 2 displays the new two-dimensional ANCF beam element.

This element is different from the Omar–Shabana beam element in that the gradient vectors of the four corner points of the plane rectangular beam element along the  $Y$  direction are used to control the position of the points in the beam. This element has 16 generalized coordinates (Fig. 2), where  $\mathbf{r}$ ,  $\mathbf{r}_X$ , and  $\mathbf{r}_Y$  are all functions with time and material coordinates  $X$  and  $Y$ . The generalized coordinate array of this element can be defined as follows:

$$\mathbf{q} = \left[ \mathbf{r}_{(0,0)}^T \quad \mathbf{r}_{X(0,0)}^T \quad \mathbf{r}_{Y(0,-\frac{h}{2})}^T \quad \mathbf{r}_{Y(0,\frac{h}{2})}^T \quad \mathbf{r}_{(L,0)}^T \quad \mathbf{r}_{X(L,0)}^T \quad \mathbf{r}_{Y(L,-\frac{h}{2})}^T \quad \mathbf{r}_{Y(L,\frac{h}{2})}^T \right]^T. \quad (7)$$

To avoid the lower-order interpolation in the transverse direction, the higher-order element has the following interpolation function, which is quadratic in the transverse direction of the beam element:

$$\mathbf{r} = \begin{bmatrix} x \\ y \end{bmatrix} = \begin{bmatrix} a_0 + a_1 X + a_2 Y + a_3 XY + a_4 X^2 + a_5 Y^2 + a_6 XY^2 + a_7 X^3 \\ b_0 + b_1 X + b_2 Y + b_3 XY + b_4 X^2 + b_5 Y^2 + b_6 XY^2 + b_7 X^3 \end{bmatrix}. \quad (8)$$

Equation (8) is not a complete polynomial, in which the missing  $X^2Y$  term can better reflect the coupling effect between axial deformation and lateral deformation of the beam,  $Y^3$  term can better capture the distribution of transverse strain  $\epsilon_y$  along the transverse direction due to the high-order interpolation in the lateral direction.

The generalized coordinates are used to describe the position of points; hence, Eq. (8) can be rewritten as follows:

$$\mathbf{r} = [S_1 \mathbf{I} \quad S_2 \mathbf{I} \quad S_3 \mathbf{I} \quad S_4 \mathbf{I} \quad S_5 \mathbf{I} \quad S_6 \mathbf{I} \quad S_7 \mathbf{I} \quad S_8 \mathbf{I}] \mathbf{q}, \quad (9)$$

where  $S_1 \sim S_8$  can be written as

$$\begin{aligned} S_1 &= 1 - 3\xi^2 + 2\xi^3 & S_2 &= L(\xi - 2\xi^2 + \xi^3) \\ S_3 &= \frac{h\eta}{2}(1 - \xi)(1 - \eta) & S_4 &= \frac{h\eta}{2}(1 - \xi)(1 + \eta) \\ S_5 &= 3\xi^2 - 2\xi^3 & S_6 &= L(-\xi^2 + \xi^3) \\ S_7 &= \frac{h\eta}{2}\xi(1 - \eta) & S_8 &= \frac{h\eta}{2}\xi(1 + \eta) \end{aligned}. \quad (10)$$

### 3.2 Inertial force

The inertial force of beam element can be determined by considering the total kinetic energy of the element and applying the Lagrange dynamic equation. The element kinetic energy  $T$  can be conventionally written as follows according to Eq. (9).

$$T = \frac{1}{2} \int_V \rho \dot{\mathbf{r}}^T \dot{\mathbf{r}} dV = \frac{1}{2} \dot{\mathbf{q}}^T \int_V \rho \mathbf{S}^T \mathbf{S} dV \dot{\mathbf{q}}. \quad (11)$$

here  $\rho$ ,  $V$ , and  $\int_V \rho \mathbf{S}^T \mathbf{S} dV$  represent the beam density, volume domain of the element in the initial configuration including the curved beam, and element mass matrix  $\mathbf{M}$  (a positive definite constant matrix), respectively. The generalized inertial force array in the ANCF can be obtained by differentiating the kinetic energy  $T$ , with respect to the time, as follows:

$$\mathbf{F} = \int_V \rho \mathbf{S}^T \mathbf{S} dV \ddot{\mathbf{q}} = \mathbf{M} \ddot{\mathbf{q}}. \quad (12)$$

### 3.3 Elastic force

The elastic force in the flexible beam element is directly related to the strain energy function. It can be expressed as the partial derivative of the strain energy in terms of the generalized coordinates:

$$\mathbf{Q}_e = \frac{\partial U}{\partial \mathbf{q}^T}. \quad (13)$$

The strain energy function can be written in a unified manner as

$$U = \frac{1}{2} \int_V \boldsymbol{\varepsilon}^T \boldsymbol{\sigma} dV = \frac{1}{2} \int_V \boldsymbol{\varepsilon}^T \mathbf{D} \boldsymbol{\varepsilon} dV. \quad (14)$$

here  $\boldsymbol{\varepsilon}$  and  $\boldsymbol{\sigma}$  are defined as arrays, which have six strain and stress components, respectively.  $\mathbf{D}$  represents the elastic coefficient matrix, and the constitutive relation used in (14) can reflect the mechanical properties of the materials. For the isotropic linear elastic materials,  $\mathbf{D}$  can be written as follows:

$$\mathbf{D} = \begin{bmatrix} \lambda + 2\mu & \lambda & \lambda & 0 & 0 & 0 \\ \lambda & \lambda + 2\mu & \lambda & 0 & 0 & 0 \\ \lambda & \lambda & \lambda + 2\mu & 0 & 0 & 0 \\ 0 & 0 & 0 & \mu & 0 & 0 \\ 0 & 0 & 0 & 0 & \mu & 0 \\ 0 & 0 & 0 & 0 & 0 & \mu \end{bmatrix}, \quad (15)$$

where  $\lambda$  and  $\mu$  represent the first and second Lamé constant, respectively.

In the case of plane stress or plane strain, the coefficient matrix takes the following forms, respectively:

$$\mathbf{D}_{\text{stress}} = \frac{E}{(1 - \mu^2)} \begin{bmatrix} 1 & \mu & 0 \\ \mu & 1 & 0 \\ 0 & 0 & \frac{1-\mu}{2} \end{bmatrix}$$

$$\mathbf{D}_{\text{strain}} = \frac{E(1 - \mu)}{(1 + \mu)(1 - 2\mu)} \begin{bmatrix} 1 & \frac{\mu}{1-\mu} & 0 \\ \frac{\mu}{1-\mu} & 1 & 0 \\ 0 & 0 & \frac{1-2\mu}{2(1-\mu)} \end{bmatrix}. \quad (16)$$

Additionally, six Green–Lagrange strain components can be written using the continuum mechanics as follows [23]:

$$\varepsilon_x = \frac{1}{2} (\|\mathbf{r}_X\|_2^2 - 1)$$

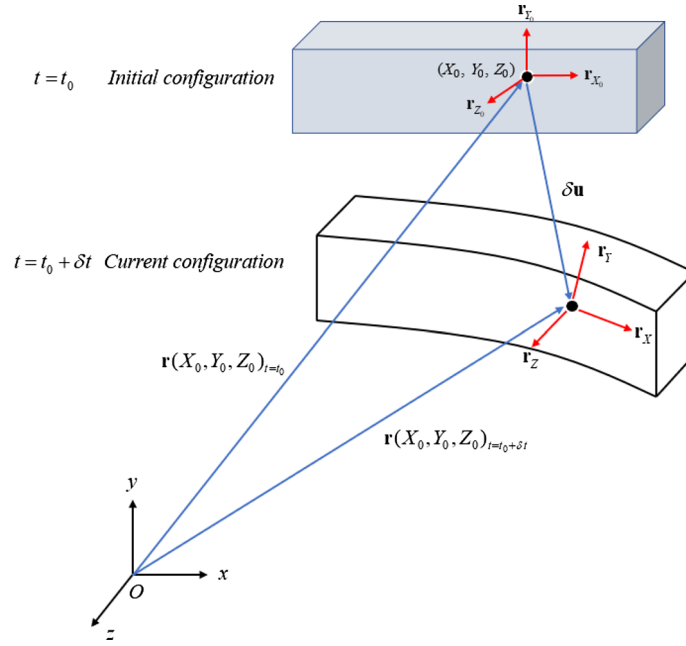


**Fig. 3** Instantaneous deformation of the element

$$\begin{aligned}
 \varepsilon_y &= \frac{1}{2} (\|\mathbf{r}_Y\|_2^2 - 1) \\
 \varepsilon_z &= \frac{1}{2} (\|\mathbf{r}_Z\|_2^2 - 1) \\
 \varepsilon_{xy} &= \frac{1}{2} \gamma_{xy} = \frac{1}{2} \mathbf{r}_X \cdot \mathbf{r}_Y \\
 \varepsilon_{xz} &= \frac{1}{2} \gamma_{xz} = \frac{1}{2} \mathbf{r}_X \cdot \mathbf{r}_Z \\
 \varepsilon_{yz} &= \frac{1}{2} \gamma_{yz} = \frac{1}{2} \mathbf{r}_Y \cdot \mathbf{r}_Z.
 \end{aligned} \tag{17}$$

### 3.4 External force and moment

Assume that the position  $(X, Y, Z)$  and its cross section are acted by the external force  $\mathbf{F}$  and moment  $\mathbf{M}$ , respectively, in which their directions are both fixed in space. Figure 3 presents the deformation of the element during the time variation  $\delta t$ .

In Fig. 3,  $\mathbf{r}_{X_0}$ ,  $\mathbf{r}_{Y_0}$ , and  $\mathbf{r}_{Z_0}$  are defined as three orthogonal gradient vectors at position  $(X_0, Y_0, Z_0)$  under the initial configuration.  $\delta \mathbf{u}(X_0, Y_0, Z_0)$  represents the virtual displacement of the point. Generally, the external virtual work  $\delta W$  generated by the external force  $\mathbf{F}$  and moment  $\mathbf{M}$  can be expressed as follows:

$$\delta W = \delta \mathbf{r}^T \mathbf{F} + \delta \Phi^T \mathbf{M}, \tag{18}$$

where  $\delta \mathbf{r}$  and  $\delta \Phi$  represent the virtual displacement and virtual rotation angle matrices on the local coordinates system, respectively. Further,  $\delta \mathbf{r}$  can be conventionally written as follows according to Eq. (3).

$$\delta \mathbf{r} = \delta \mathbf{u} = \mathbf{S}_{(X_0, Y_0, Z_0)} \delta \mathbf{q}. \tag{19}$$

Additionally, the matrix of direction cosine between the different coordinate base vectors can be used to represent the virtual rotation angle vector of the beam cross section. The angular velocity vector of instantaneous rotation at this point can be written as:

$$\boldsymbol{\omega} = (\dot{\mathbf{e}}_2 \cdot \mathbf{e}_3) \mathbf{e}_1 + (\dot{\mathbf{e}}_3 \cdot \mathbf{e}_1) \mathbf{e}_2 + (\dot{\mathbf{e}}_1 \cdot \mathbf{e}_2) \mathbf{e}_3, \tag{20}$$

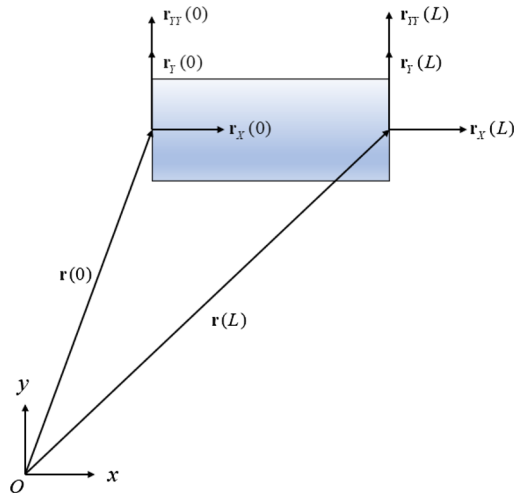


**Fig. 4** Patel–Shabana beam element

where  $\mathbf{e}_1$ ,  $\mathbf{e}_2$ , and  $\mathbf{e}_3$  represent the base vectors of local coordinate system. Furthermore,  $\frac{\mathbf{r}_x}{\|\mathbf{r}_x\|}$  can be used instead of  $\mathbf{e}_1$ ,  $\frac{\mathbf{r}_y}{\|\mathbf{r}_y\|}$  can be used instead of  $\mathbf{e}_2$ , and  $\frac{\mathbf{r}_z}{\|\mathbf{r}_z\|}$  can be used instead of  $\mathbf{e}_3$ . So, the instantaneous virtual rotation angle vector can be obtained by substituting the relevant expressions into the variational equation of angular velocity, which can be obtained from Eq. (20). The specific expression is as follows:

$$\delta\Phi = \frac{\delta\mathbf{r}_Y^T \mathbf{r}_Z}{\|\mathbf{r}_Y\|_2 \cdot \|\mathbf{r}_Z\|_2} \mathbf{e}_1 + \frac{\delta\mathbf{r}_Z^T \mathbf{r}_X}{\|\mathbf{r}_Z\|_2 \cdot \|\mathbf{r}_X\|_2} \mathbf{e}_2 + \frac{\delta\mathbf{r}_X^T \mathbf{r}_Y}{\|\mathbf{r}_X\|_2 \cdot \|\mathbf{r}_Y\|_2} \mathbf{e}_3, \quad (21)$$

Based on Eqs. (19) and (21), the generalized external force can be expressed as follows:

$$\tilde{\mathbf{F}} = \mathbf{S}^T \mathbf{F} + \left[ \frac{\mathbf{S}_Y^T \mathbf{r}_Z}{\|\mathbf{r}_Y\|_2 \cdot \|\mathbf{r}_Z\|_2} \quad \frac{\mathbf{S}_Z^T \mathbf{r}_X}{\|\mathbf{r}_Z\|_2 \cdot \|\mathbf{r}_X\|_2} \quad \frac{\mathbf{S}_X^T \mathbf{r}_Y}{\|\mathbf{r}_X\|_2 \cdot \|\mathbf{r}_Y\|_2} \right] \mathbf{M}. \quad (22)$$

#### 4 Patel–Shabana beam element

This section introduces a higher-order planar beam element developed by Patel and Shabana. This element has demonstrated its effectiveness in alleviating Poisson locking. The element interpolation polynomial, which is quadratic in the transverse direction of the beam, is consistent with Eq. (8). Figure 4 displays the element.

Unlike the traditional Omar–Shabana beam element, the proposed element incorporates that a higher-order curvature vector  $\mathbf{r}_{yy}$  is used to capture the beam transverse deformation. The generalized coordinates array of this element can be defined as follows:

$$\mathbf{q} = \left[ \mathbf{r}_{(0,0)}^T \quad \mathbf{r}_{X(0,0)}^T \quad \mathbf{r}_{Y(0,0)}^T \quad \mathbf{r}_{YY(0,0)}^T \quad \mathbf{r}_{(L,0)}^T \quad \mathbf{r}_{X(L,0)}^T \quad \mathbf{r}_{Y(L,0)}^T \quad \mathbf{r}_{YY(L,0)}^T \right]. \quad (23)$$

Additionally, the position vector of any material point in the beam can be expressed as in Eq. (9), whereas the derived element shape function, different from Eq. (10), can be expressed as follows:

$$\begin{aligned} S_1 &= 1 - 3\xi^2 + 2\xi^3 & S_2 &= L(\xi - 2\xi^2 + \xi^3) \\ S_3 &= h(1 - \xi)\eta & S_4 &= \frac{h^2\eta^2}{2}(1 - \xi) \\ S_5 &= 3\xi^2 - 2\xi^3 & S_6 &= L(-\xi^2 + \xi^3) \\ S_7 &= h\xi\eta & S_8 &= \frac{h^2\eta^2}{2}\xi \end{aligned}, \quad (24)$$

where  $\xi = \frac{X}{L}$ ,  $\eta = \frac{Y}{h}$ , and the definitions of  $L$  and  $h$  are the same as that mentioned above. To gain a clearer understanding of the mechanical mechanism and differences in alleviating Poisson locking between the ANCF element proposed in Sect. 3 and this higher-order planar beam element, the distribution characteristics of

transverse strain  $\varepsilon_y$  on the cross section at position  $X = 0$  are further investigated. For this higher-order planar beam element, the transverse strain  $\varepsilon_y$  can be expressed as follows according to Eq. (5):

$$\varepsilon_y = \frac{1}{2}[(k_5 + \eta hk_7)^2 + (k_6 + \eta hk_8)^2 - 1]. \quad (25)$$

here  $k_5$  and  $k_6$  represent the two components of the gradient vector  $\mathbf{r}_Y(0)$  in the global coordinate system, respectively, and  $k_7$  and  $k_8$  represent the two components of the curvature vector  $\mathbf{r}_{YY}(0)$  in the global coordinate system. Thus, if the gradient vector  $\mathbf{r}_y$  at any position in the cross section ( $X = 0$ ) is Taylor expanded at the coordinate origin  $(0, 0)$ , Eq. (26) can be obtained as follows:

$$\begin{aligned} \mathbf{r}_Y|_{(X,Y)=(0,\eta h)} &= \mathbf{r}_Y|_{(X,Y)=(0,0)} + \mathbf{r}_{YY}|_{(X,Y)=(0,0)}\eta h \\ &= \begin{bmatrix} k_5 \\ k_6 \end{bmatrix} + \begin{bmatrix} k_7 \\ k_8 \end{bmatrix} \eta h. \end{aligned} \quad (26)$$

Equation (26) only retains the linear term of Taylor expansion. The transverse strain  $\varepsilon_y$  depends on the gradient vector  $\mathbf{r}_Y$  according to Eq. (5). This highly nonlinear gradient vector  $\mathbf{r}_Y$  is linearly expressed using Taylor expansion at origin position  $(0, 0)$ , as expressed in Eq. (25). Thus, the Patel–Shabana beam element can capture higher-order transverse deformation, resulting in its ability to alleviate Poisson locking.

Correspondingly, the proposed ANCF beam element has the same number of generalized coordinates as that of the Patel–Shabana beam, but it has different generalized coordinate types. The new element lacks curvature vector  $\mathbf{r}_{YY}$ , which is replaced by four gradient vectors, namely,  $\mathbf{r}_Y(0, \frac{h}{2})$ ,  $\mathbf{r}_Y(0, -\frac{h}{2})$ ,  $\mathbf{r}_Y(L, \frac{h}{2})$ ,  $\mathbf{r}_Y(L, -\frac{h}{2})$ , located at corner points. The transverse strain  $\varepsilon_y(X = 0)$  can be similarly expressed as follows:

$$\begin{aligned} \varepsilon_y &= \frac{1}{2}(\delta_x^2 + \delta_y^2 - 1) \\ \delta_x &= k'_5 \left( \frac{1}{2} - \eta \right) + k'_7 \left( \frac{1}{2} + \eta \right) \\ \delta_y &= k'_6 \left( \frac{1}{2} - \eta \right) + k'_8 \left( \frac{1}{2} + \eta \right). \end{aligned} \quad (27)$$

here  $k'_5$  and  $k'_6$  represent the two components of the gradient vector  $\mathbf{r}_Y(0, -\frac{h}{2})$  in the global coordinate system, respectively, and  $k'_7$  and  $k'_8$  represent the two components of the curvature vector  $\mathbf{r}_Y(0, \frac{h}{2})$  in the global coordinate system, respectively. Note that, due to the use of four corner gradient vectors in Sect. 3, this highly nonlinear gradient vector  $\mathbf{r}_Y$  is linearly expressed using the linear interpolation of boundary points, as expressed in Eq. (27). Generally, the high-order curvature vector  $\mathbf{r}_{YY}$  is used in the Patel–Shabana beam element to linearize  $\mathbf{r}_Y$  based on Taylor expansion. However, the proposed ANCF beam element uses gradient vectors of corner points, rather than curvature vectors, to linearize  $\mathbf{r}_Y$  based on numerical interpolation. These two different improved methods can enable the ANCF element to capture the deformation characteristics of the cross section, especially transverse deformation.

### 5 Three-dimensional spatial beam element

Three-dimensional form of the new two-dimensional shear deformable ANCF beam element proposed in Sect. 3 is discussed in this section to generalize this method. Accordingly, the interpolation functions used to describe the spatial position of material points can be defined as follows:

$$\mathbf{r} = \begin{bmatrix} x \\ y \\ z \end{bmatrix} = \begin{bmatrix} a_0 + a_1 X + a_2 Y + a_3 Z + a_4 XY + a_5 XZ + a_6 X^2 + a_7 Y^2 + a_8 Z^2 \\ + a_9 XY^2 + a_{10} XZ^2 + a_{11} X^3 \\ b_0 + b_1 X + b_2 Y + b_3 Z + b_4 XY + b_5 XZ + b_6 X^2 + b_7 Y^2 + b_8 Z^2 \\ + b_9 XY^2 + b_{10} XZ^2 + b_{11} X^3 \\ c_0 + c_1 X + c_2 Y + c_3 Z + c_4 XY + c_5 XZ + c_6 X^2 + c_7 Y^2 + c_8 Z^2 \\ + c_9 XY^2 + c_{10} XZ^2 + c_{11} X^3 \end{bmatrix}. \quad (28)$$



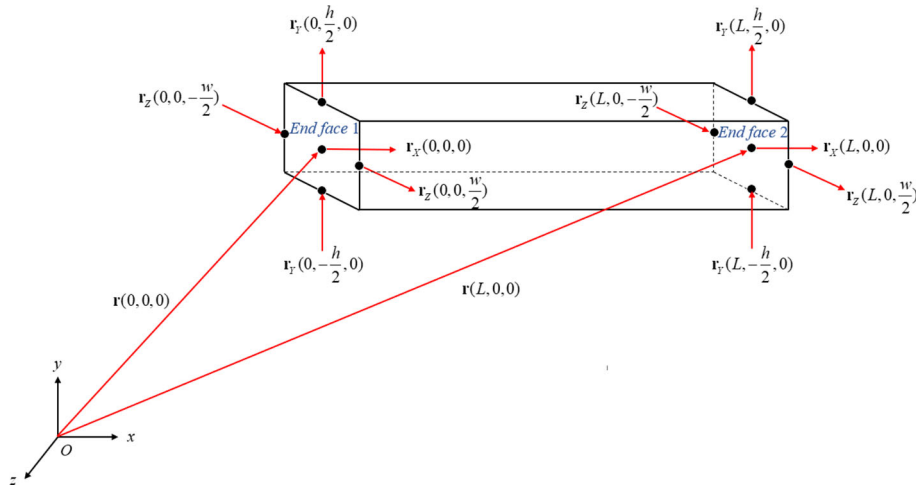


**Fig. 5** New three-dimensional ANCF beam element

Figure 5 presents the schematic diagram of the 3D ANCF beam element.

In Fig. 5, the element has 36 generalized coordinates, and the vector of the nodal coordinates of left-end face 1 for the new three-dimensional higher-order element is expressed as follows:

$$\mathbf{q}^{\text{Left}} = \left[ \mathbf{r}_{(0,0,0)}^T \quad \mathbf{r}_{X(0,0,0)}^T \quad \mathbf{r}_{Y(0,-\frac{h}{2},0)}^T \quad \mathbf{r}_{Y(0,\frac{h}{2},0)}^T \quad \mathbf{r}_{Z(0,0,-\frac{w}{2})}^T \quad \mathbf{r}_{Z(0,0,\frac{w}{2})}^T \right]^T. \quad (29)$$

here  $L, h$ , and  $w$  represent the length, height, and width of the beam element, respectively. Similarly, the element shape function  $S_1 \sim S_{12}$  can be expressed as follows, according to the corresponding generalized coordinates:

$$\begin{aligned} S_1 &= 1 - 3\xi^2 + 2\xi^3 & S_2 &= L(\xi - 2\xi^2 + \xi^3) \\ S_3 &= \frac{h\eta}{2}(1 - \xi)(1 - \eta) & S_4 &= \frac{h\eta}{2}(1 - \xi)(1 + \eta) \\ S_5 &= \frac{w\zeta}{2}(1 - \xi)(1 - \zeta) & S_6 &= \frac{w\zeta}{2}(1 - \xi)(1 + \zeta) \\ S_7 &= 3\xi^2 - 2\xi^3 & S_8 &= L(-\xi^2 + \xi^3) \\ S_9 &= \frac{h\eta}{2}\xi(1 - \eta) & S_{10} &= \frac{h\eta}{2}\xi(1 + \eta) \\ S_{11} &= \frac{w\zeta}{2}\xi(1 - \zeta) & S_{12} &= \frac{w\zeta}{2}\xi(1 + \zeta) \end{aligned} \quad (30)$$

## 6 Numerical examples

To demonstrate the effective alleviation of Poisson locking in beams, this section compares the performance of several different ANCF elements. Specifically, the Omar–Shabana, Patel–Shabana, and Shen higher-order beam elements all are considered for discussion and comparison. Thus, seven numerical examples are investigated, namely, four static analysis examples and three dynamic analysis examples. The first static example involves a slender cantilever beam with small deformations under a shearing force. The second static example considers a slender cantilever beam with small deformations under a bending moment. The last static example examines a thick cantilever beam with large deformations under a shearing force. The first dynamic example considers a cantilever beam structure under gravity loading. The second dynamic example involves a beam pendulum under gravity loading. The last dynamic example examines a spin-up cantilever beam under a moment. Additionally, new element (NE) refers to the proposed ANCF element for the convenience of description.

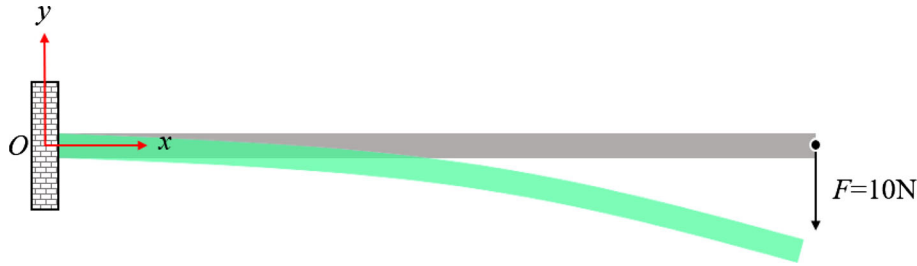


**Fig. 6** Slender cantilever beam under a shearing force

**Table 1** Basic parameters of the beam (slender cantilever beam)

Description	Value
Length/m	1
Width/m	0.01
Height/m	0.01
Young's modulus/Pa	$2 \times 10^{11}$
Poisson's ratio	0.3

**Table 2** Beam tip vertical displacement (m) in different ANCF elements (slender cantilever beam subject to shearing force)

Type	5 elements	10 elements	20 elements	50 elements	100 elements
Om–Sh	– 0.01797943	– 0.01814821	– 0.01818387	– 0.01819351	– 0.01819488
Shen	– 0.01968086	– 0.01992459	– 0.01997648	– 0.01999060	– 0.01999262
Pat–Sh	– 0.01972723	– 0.01993645	– 0.01997963	– 0.01999125	– 0.01999290
NE	– 0.01975106	– 0.01993731	– 0.01997966	– 0.01999125	– 0.01999290
Analytical	– 0.02				

## 6.1 Static examples

### 6.1.1 Slender beam subject to shearing force: small deformation

A slender cantilever beam subjected to shearing force  $F$  at its free end is considered (Fig. 6). Table 1 presents the basic parameters of the beam.

The force direction is vertical with the value of 10 N (Fig. 6). Accordingly, the slender beam deflection at the free end is calculated to be  $-0.02$  m, based on the classical Euler–Bernoulli beam theory.

Table 2 presents the numerical calculation results for the static analysis. It shows the converged beam tip vertical displacement with several different ANCF elements. Figure 7 displays the NE's iterative convergence situation. From these results, the Om–Sh beam element cannot converge to the correct solution due to excessive stiffness caused by Poisson locking, whereas the other elements can converge correctly. Specifically, the elements' convergence can be enhanced with an increase of the element division number. Moreover, the number of generalized coordinates of the NE is less, and the cost of the numerical calculation is lower, but the accuracy is higher. As shown in Fig. 7, the NE's displacement iteration can immediately converge to the exact solution.

### 6.1.2 Slender beam subjected to bending moment: small deformation

A slender cantilever beam subjected to the bending moment  $M$  at its free end is considered (Fig. 8). Table 1 presents the basic parameters of the beam.

The bending moment  $M$  is perpendicular to the  $x$ – $y$  plane with the value of 10 N m. According to the classical Euler–Bernoulli beam theory, the slender beam deflection at the free end is calculated to be  $-0.03$  m. Table 3 presents the numerical calculation results for the static analysis, and Fig. 9 shows the NE's iterative convergence situation. From these results, the Om–Sh beam element cannot converge to the correct solution either due to Poisson locking, whereas the other elements can converge correctly. Moreover, the NE does not

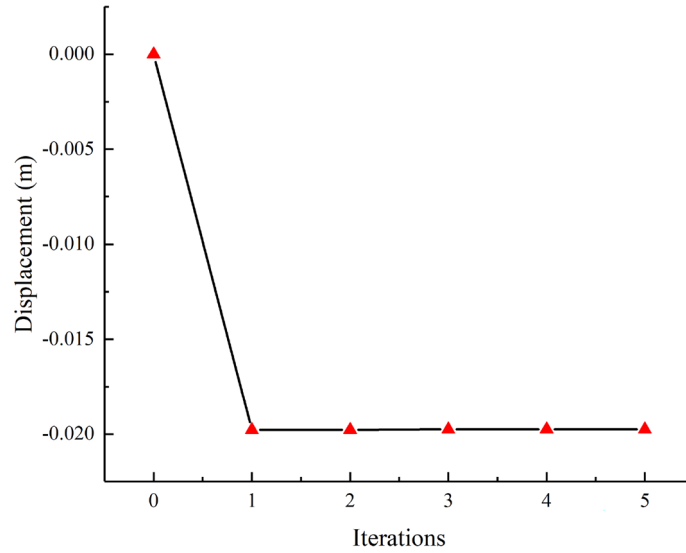


Fig. 7 Displacement iterative curve (slender beam subject to shearing force)

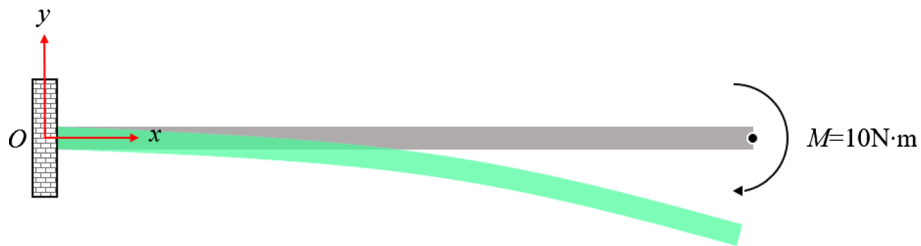


Fig. 8 Slender cantilever beam subject to the bending moment

Table 3 Beam tip vertical displacement (m) in different ANCF elements (slender cantilever beam subject to bending moment)

Type	5 elements	10 elements	20 elements	50 elements	100 elements
Om–Sh	– 0.02723433	– 0.02729156	– 0.02729456	– 0.02729474	– 0.02729475
Shen	– 0.02989644	– 0.02998744	– 0.02999225	– 0.02999257	– 0.02999270
Pat–Sh	– 0.02990484	– 0.02998794	– 0.02999232	– 0.02999258	– 0.02999262
NE	– 0.02993395	– 0.02998889	– 0.02999234	– 0.02999258	– 0.02999262
Analytical	– 0.03				

show excessive stiff mechanical behavior, indicating that the NE cannot suffer the locking, including Poisson and shear locking. Similarly, the NE’s displacement iteration can converge to the exact solution soon (Fig. 9).

6.1.3 Thick beam subjected to shearing force: large deformation

A thick beam example (Fig. 10) is used to investigate the elements’ convergence under large deformation. The left-end face of the beam is completely consolidated with ground, whereas a vertical force with  $1 \times 10^8$  N is applied to the free end. Table 4 presents the basic parameters of the beam. To compare with the convergent solution of the ANCF elements, the reference displacement solution of  $-0.19560853$  m is calculated using the commercial finite element code in this section.

Table 5 indicates that the Om–Sh beam element converges to an incorrect solution, which is smaller than the reference solution due to excessive stiffness caused by Poisson locking. The other elements’ displacement solutions are closer to the reference solution with the increase of element divisions number. This observation also demonstrates that the NE effectively alleviates Poisson locking, particularly under the condition of large static deformation.

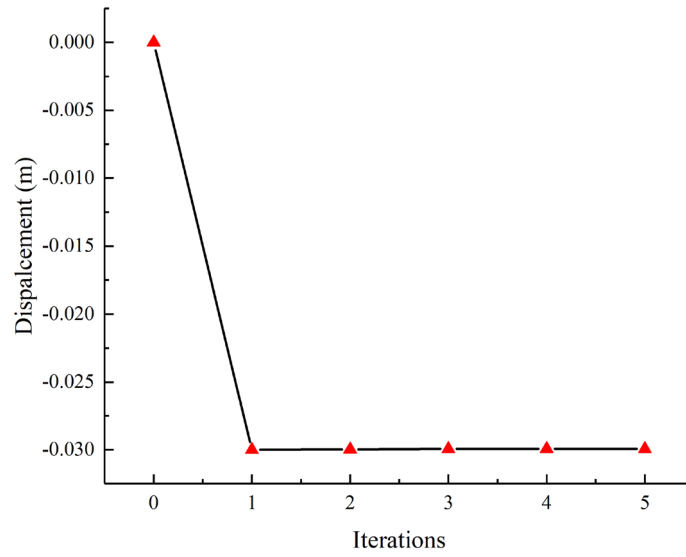


**Fig. 9** Displacement iterative curve (slender beam subject to bending moment)

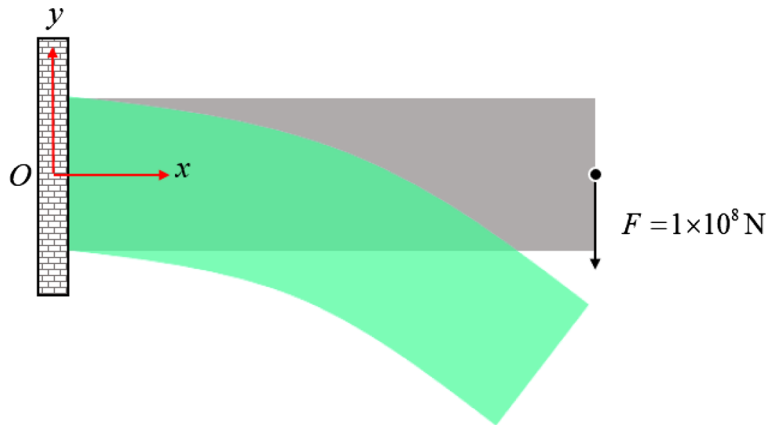


**Fig. 10** Thick beam subjected to shearing force

**Table 4** Basic parameters of the beam (thick beam)

Description	Value
Length/m	1
Width/m	0.1
Height/m	0.5
Young's modulus /Pa	$2 \times 10^{11}$
Poisson's ratio	0.3

**Table 5** Beam tip vertical displacement (m) in different ANCF elements (thick beam subjected to shearing force)

Type	5 elements	10 elements	20 elements	50 elements	100 elements
Om-Sh	-0.17082478	-0.17225318	-0.17271488	-0.17291039	-0.17296168
Shen	-0.18892794	-0.19189735	-0.19320325	-0.19394511	-0.19419846
Pat-Sh	-0.18830649	-0.19076078	-0.19177493	-0.19228740	-0.19245055
NE	-0.18888512	-0.19137023	-0.19237288	-0.19287577	-0.19303419
ABAQUS	-0.19560853				

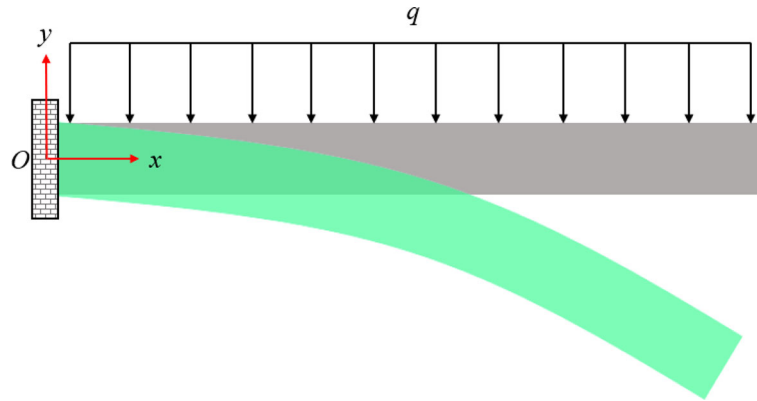


**Fig. 11** Cantilever beam subjected to the gravity loading

**Table 6** Basic parameters of the beam (cantilever beam)

Description	Value
Length/m	1
Width/m	0.1
Height/m	0.1
Density/kg m <sup>-3</sup>	5000
Young's modulus/Pa	5 × 10 <sup>7</sup>
Poisson's ratio	0.3

**Table 7** Basic parameters of the beam (beam pendulum)

Description	Value
Length/m	1
Width/m	0.1
Height/m	0.01
Density/kg m <sup>-3</sup>	7750
Young's modulus/Pa	2 × 10 <sup>6</sup>
Poisson's ratio	0.3

## 6.2 Dynamic examples

### 6.2.1 Cantilever beam

This section introduces a dynamic problem involving a cantilever beam subjected to gravity loading as an external force. The purpose of this problem is to demonstrate that the ability of the proposed NE element in effectively alleviating locking phenomena in dynamic simulations. The cantilever beam was subjected to gravity loading  $q$  (Fig. 11). Table 6 presents the basic parameters of the beam.

Figures 12 and 13 show the curves of the horizontal and vertical positions of the beam tip with time, respectively. The Om–Sh element exhibits a significant locking mechanical behavior as evidenced by its notably small tip displacement. Meanwhile, the beam tip displacement results of Shen, Pat–Sh, and NE elements are closely aligned, indicating a more accurate representation of the actual solution and reflecting the desired characteristics.

### 6.2.2 Beam pendulum

To further investigate the influence of the locking phenomenon on these ANCF elements, a dynamic beam pendulum problem is presented in this section. The beam pendulum was subjected to gravity loading  $q$  (Fig. 14). Table 7 presents the basic parameters of the beam.

Figures 15 and 16 display the curves of the horizontal and vertical positions of the beam tip with time, respectively. The displacement results of the Om–Sh element are not much different from those of the other

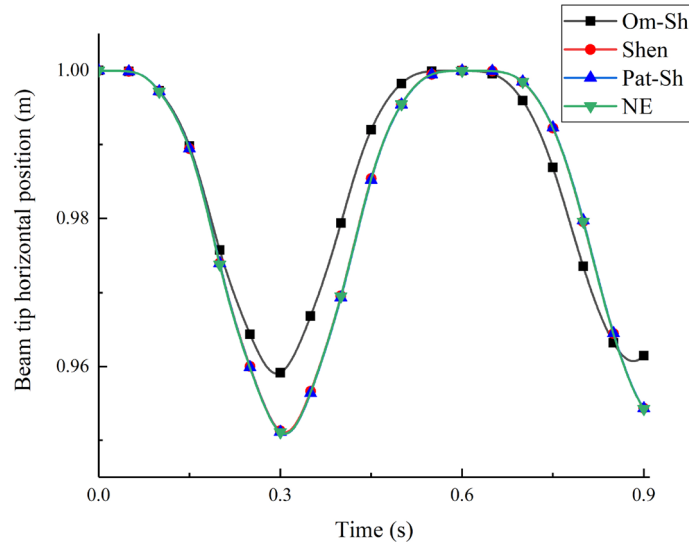


**Fig. 12** Comparison of the beam tip horizontal position for different elements (cantilever beam)

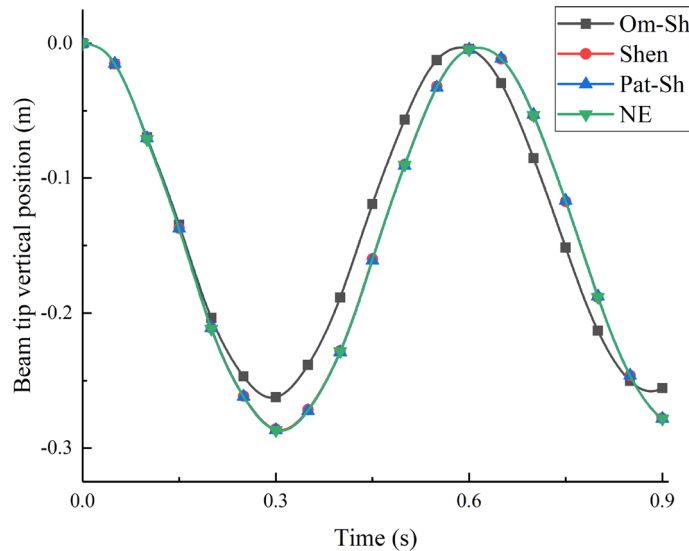


**Fig. 13** Comparison of the beam tip vertical position for different elements (cantilever beam)

three high-order elements. The reason is that the elastic deformation caused by incorrect cross-sectional strain distribution has less influence on the overall displacement of the element than the large-scale rigid displacement of the beam pendulum. Additionally, the Om-Sh element displacement solution is highly consistent with that of Shen and Pat-Sh element, demonstrating the effectiveness of the proposed element in alleviating locking.

### 6.2.3 Spin-up beam

This section presents a spin-up beam dynamic problem to demonstrate that the newly proposed ANCF element (NE) can effectively help alleviate locking in the process of rapid rotation. The left end, where a constant moment with 50 N is applied, is connected with the ground through the spherical joint, and the right side is free (Fig. 17). Table 8 presents the basic parameters of the beam.

Figures 18 and 19 present the comparison of the tip horizontal and vertical displacement solutions with Pat-Sh and NE, respectively. The results indicate good consistency and convergence between the two different ANCF elements for dynamic analysis.

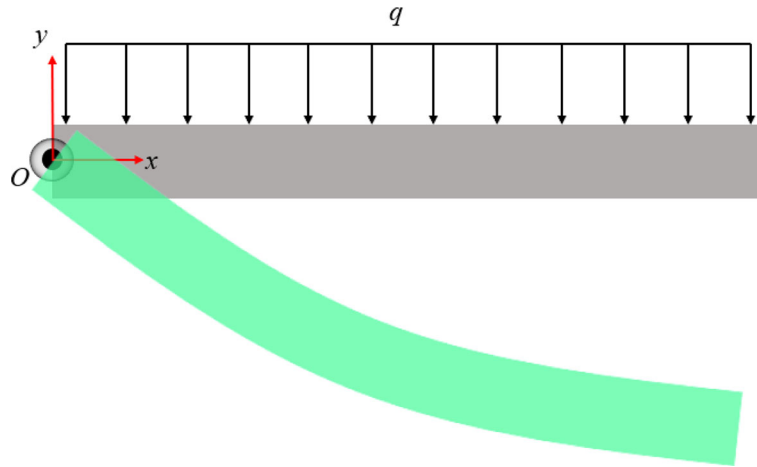


Fig. 14 Beam pendulum

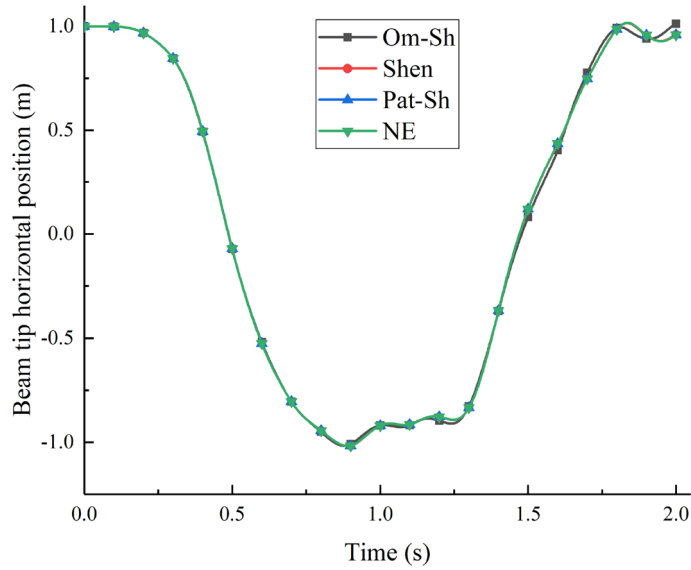


Fig. 15 Comparison of the beam tip horizontal position for different elements (beam pendulum)

Table 8 Basic parameters of the beam (beam pendulum)

Description	Value
Length/m	1
Width/m	0.1
Height/m	0.01
Density/kg m <sup>-3</sup>	7800
Young's modulus/Pa	2 × 10 <sup>8</sup>
Poisson's ratio	0.3

### 7 Conclusions

The transverse  $\varepsilon_y$  can be more accurately captured by using multiple gradient vectors in the cross section. Accordingly, a new finite element was developed using the absolute nodal coordinate formulation. The efficiency of the new element in alleviating locking was demonstrated through the analysis of three static problems, showing comparable performance to the Shen and Pat–Sh beam elements. However, unlike the Shen element relies on numerous generalized coordinates and Pat–Sh element that introduces a high-order curva-

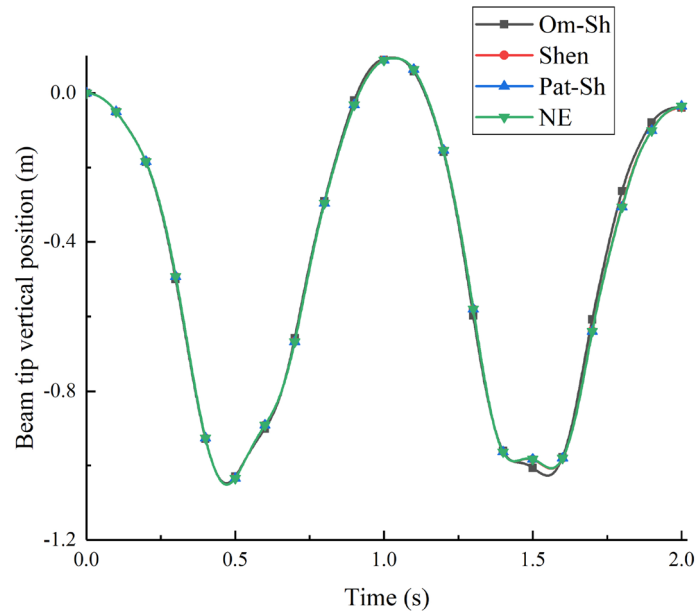


Fig. 16 Comparison of the beam tip vertical position for different elements (beam pendulum)



Fig. 17 Spin-up beam

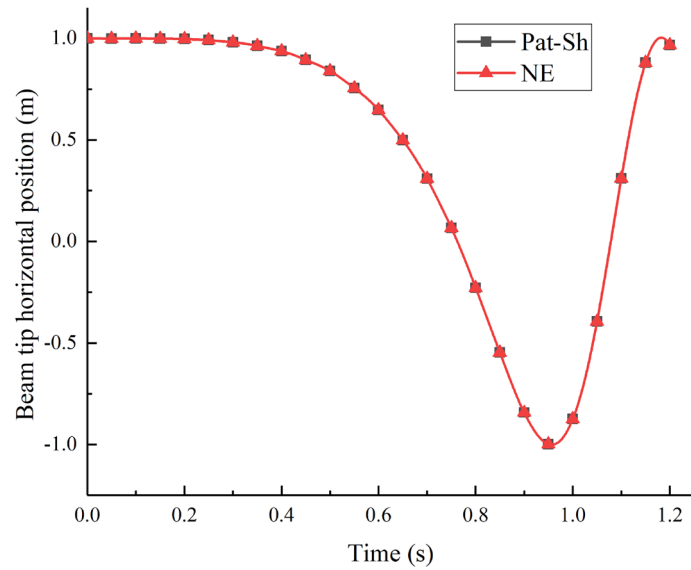
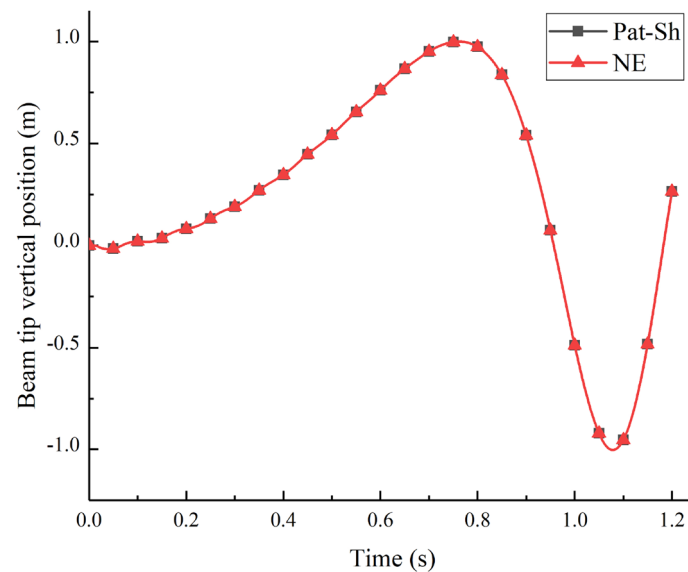


Fig. 18 Comparison of the beam tip horizontal position for different elements (spin-up beam)





**Fig. 19** Comparison of the beam tip vertical position for different elements (spin-up beam)

ture vector, the proposed element features a reduced number of generalized coordinates. Consequently, its numerical iterative calculations are faster and yield higher accuracy. Additionally, three dynamic problems were used to demonstrate the effectiveness of the proposed element in alleviating locking in complex dynamic behaviors (e.g., cantilever beam, beam pendulum, and spin-up beam). First, in the dynamic cantilever beam problem, a notable difference is observed in the beam tip displacement between the proposed element (NE) and Om–Sh element, indicating that the NE can effectively alleviate locking phenomena in dynamic scenarios. Second, in the beam pendulum problem, the results are not significantly different between the Om–Sh element and the other three high-order elements since the beam motion is mainly rigid in a large range. Finally, the study provides further confirmation of the adaptability, rationality, and effectiveness of the proposed ANCF beam element since the tip displacement results of the propose element and Pat–Sh exhibit a high degree of consistency in the spin-up beam problem.

**Author contributions** MZ performed investigation and writing—original draft. MT performed writing—review and editing. JC performed validation. LL contributed to conceptualization.

**Data availability** The datasets generated and analyzed during the current study are available from the corresponding author on reasonable request.

## Declarations

**Conflict of interest** The authors have no relevant financial or non-financial interests to disclose.

## References

1. Shabana, A.A.: Flexible multibody dynamic: review of past and recent developments. *Multibody Syst. Dyn.* **1**(2), 189–222 (1997)
2. Shabana, A.A.: Definition of the slopes and absolute nodal coordinate formulation. *Multibody Syst. Dyn.* **1**, 339–348 (1997)
3. Shabana, A.A.: *Dynamics of Multibody Systems*, 4th edn. Cambridge University Press, Cambridge (2013)
4. Omar, M.A., Shabana, A.A.: A two-dimensional shear deformable beam for large rotation and deformation problems. *J. Sound Vib.* **243**(3), 565–576 (2001)
5. Garcia-Vallejo, D., Mikkola, A.M., Escalona, J.L.: A new locking-free shear deformable finite element based on absolute nodal coordinates. *Nonlinear Dyn.* **50**(1–2), 249–264 (2007)
6. Sapanen, J.T., Mikkola, A.: Description of elastic forces in absolute nodal coordinate formulation. *Nonlinear Dyn.* **34**(1), 53–74 (2003)

7. Gerstmayr, J., Matikainen, M.K., Mikkola, A.M.: A geometrically exact beam element based on the absolute nodal coordinate formulation. *Multibody Syst. Dyn.* **20**(4), 359–384 (2008)
8. Gerstmayr, J., Schöberl, J.: A 3D finite element method for flexible multibody systems. *J. Multibody Syst. Dyn.* **15**, 309–324 (2006)
9. Gerstmayr, J., Shabana, A.A.: Analysis of thin beams and cables using the absolute nodal coordinate formulation. *Nonlinear Dyn.* **45**(1–2), 109–130 (2006)
10. Hurskainen, V.V.T., Matikainen, M.K., Wang, J.J., Mikkola, A.M.: A planar beam finite-element formulation with individually interpolated shear deformation. *ASME J. Comput. Nonlinear Dyn.* **12**(4), 041007 (2016)
11. Schwab, A.L., Meijaard, J.P.: Comparison of three-dimensional flexible beam elements for dynamic analysis: finite element method and absolute nodal coordinate formulation. In: *Proceedings of the IDETC/CIE 2005 Long Beach, New York, USA*, September 24–28 (2005)
12. Nachbagauer, K., Pechstein, A.S., Irschik, H., Gerstmayr, J.: A new locking-free formulation for planar, shear deformable, linear and quadratic beam finite elements based on the absolute nodal coordinate formulation. *Multibody Syst. Dyn.* **26**(3), 245–263 (2011)
13. Nachbagauer, K., Gruber, P., Gerstmayr, J.: Structural and continuum mechanics approaches for a 3D shear deformable ANCF beam finite element: application to static and linearized dynamic examples. *ASME J. Comput. Nonlinear Dyn.* **8**(2), 021004-1–021004-7 (2013)
14. Shen, Z., Li, P., Liu, C., Hu, G.: A finite element beam model including cross-section distortion in the absolute nodal coordinate formulation. *Nonlinear Dyn.* **77**(3), 1019–1033 (2014)
15. Shen, Z., Xing, X., Li, B.: A new thin beam element with cross-section distortion of the absolute nodal coordinate formulation. *Proc. Inst. Mech. Eng. Part C J. Mech. Eng. Sci.* **235**(24), 7456–7467 (2021)
16. Orzechowski, G., Shabana, A.A.: Analysis of warping deformation modes using higher-order ANCF beam element. *J. Sound Vib.* **363**, 428–445 (2016)
17. Patel, M., Shabana, A.A.: Locking alleviation in the large displacement analysis of beam elements: the strain split method. *Acta Mech.* **229**(7), 2923–2946 (2018)
18. Shabana, A.A., Desai, C.J., Grossi, E., Patel, M.: Generalization of the strain-split method and evaluation of the nonlinear ANCF finite elements. *Acta Mech.* **231**(4), 1365–1376 (2020)
19. Shaukat, A.R., Lan, P., Wang, J., Wang, T.: In-plane nonlinear postbuckling analysis of circular using absolute nodal coordinate formulation with arc-length method. *Proc. Inst. Mech. Eng. Part K J. Multi-Body Dyn.* **235**(3), 297–311 (2021)
20. Tang, H., Zhang, Z., Liu, C., Liu, S.: Locking alleviation techniques of two types of beam elements based on the local frame formulation. *Chin. J. Theor. Appl. Mech.* **53**(2), 482–495 (2021)
21. Shabana, A.A.: An overview of the ANCF approach, justifications for its use, implementation issues, and future research directions. *Multibody Syst. Dyn.* (2023). <https://doi.org/10.1007/s11044-023-09890-z>
22. Zhang, D.Y., Luo, J.J., Wang, H., Ma, X.F.: Locking problem and locking alleviation of ANCF/CRBF planar beam elements. *Chin. J. Theor. Appl. Mech.* **53**(3), 874–889 (2021)
23. Shabana, A.A.: *Computational Continuum Mechanics*, 3rd edn. Wiley, Chichester (2018)

**Publisher's Note** Springer Nature remains neutral with regard to jurisdictional claims in published maps and institutional affiliations.

Springer Nature or its licensor (e.g. a society or other partner) holds exclusive rights to this article under a publishing agreement with the author(s) or other rightsholder(s); author self-archiving of the accepted manuscript version of this article is solely governed by the terms of such publishing agreement and applicable law.